

Supporting information available for

End-functionalization of dithiarubicene: Modulation of optoelectronic properties by metal-catalyzed coupling reactions and device application

Kenji Tsukamoto, Koji Takagi, Keitaro Yamamoto, Yutaka Ie, and Takanori Fukushima

Table of contents

S1. Theoretical calculation2
S2. Optoelectronic properties3
S3. OFET characteristics7
S4. OPV characteristics10
S5. NMR spectra12
S6. Reference18

S1. Theoretical calculation¹

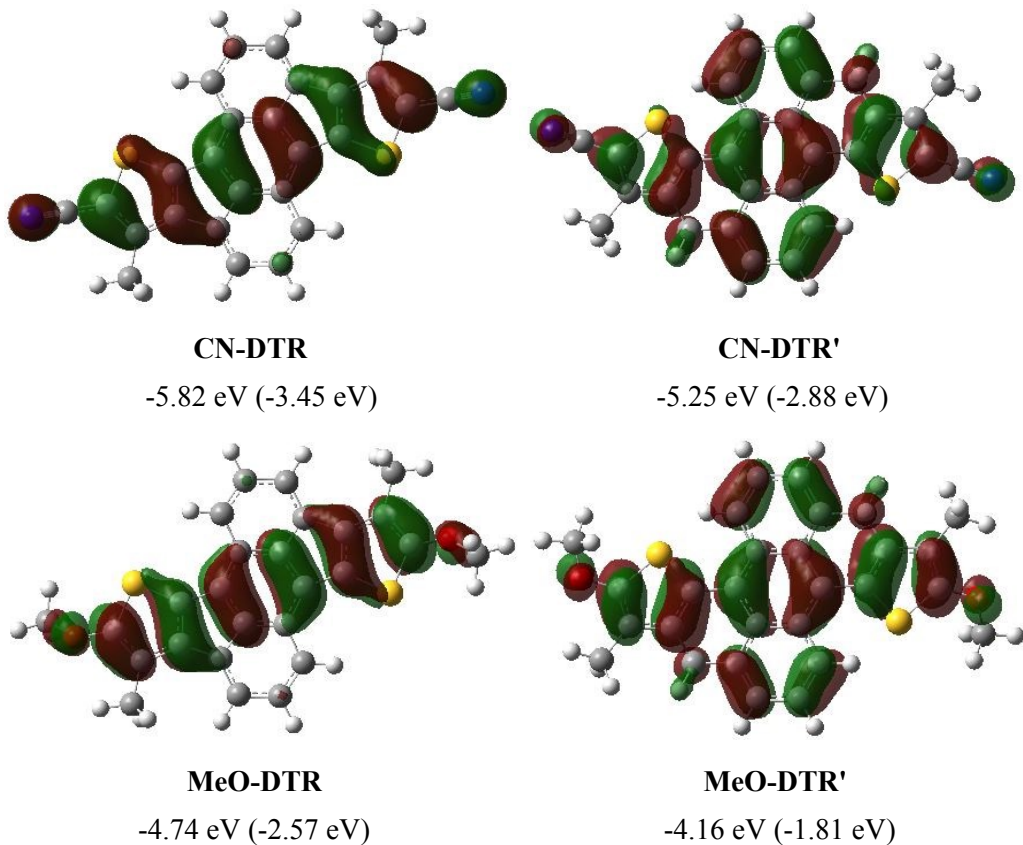


Figure S1. HOMO surfaces of dithiarubicene derivatives having the fused five-membered ring (**CN-DTR** and **MeO-DTR**, left) and virtual reference compounds having the six-membered ring (**CN-DTR'** and **MeO-DTR'**, right). The numbers indicate energy levels of HOMO and LUMO (in parenthesis) based on the DFT calculation using a B3LYP density functional and a 6-31G(d,p) basis set.

Table S1. HOMO and LUMO energy levels of five DTR derivatives.^a

	Ethyneyl- DTR	Th-DTR	Py-DTR	CN-DTR	MeO-DTR
LUMO (eV)	-2.89	-2.77	-2.98	-3.45	-2.57
HOMO (eV)	-5.01	-4.87	-5.24	-5.82	-4.74

[a] Based on the DFT calculation using a B3LYP density functional and a 6-31G(d,p) basis set.

S2. Optoelectronic properties

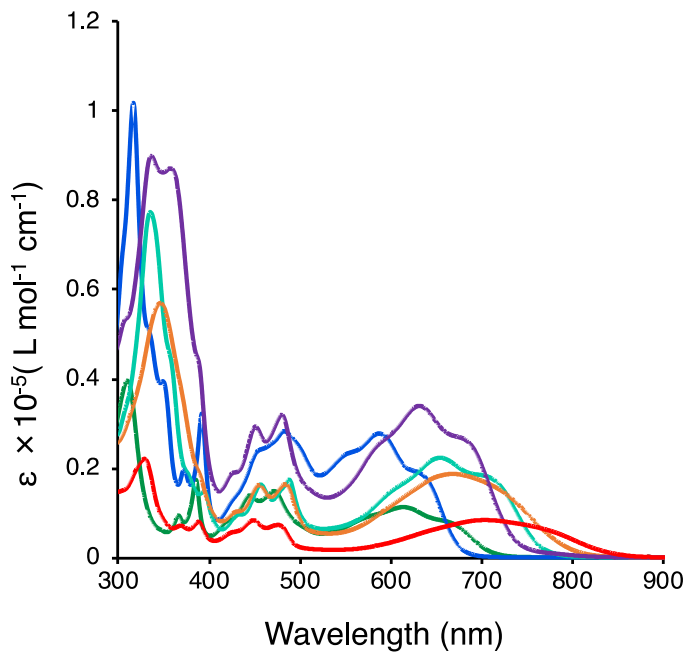


Figure S2. UV-Vis-NIR absorption spectra of **DTR** (green line), **CN-DTR** (blue line), **Py-DTR** (purple line), **Ethynyl-DTR** (light green line), **Th-DTR** (orange line), and **MeO-DTR** (red line) in CHCl₃ solution (10⁻⁵ M).

Table S2. Comparison of absorption bands between the observed value and theoretical value estimated by TD-DFT calculation (B3LYP/6-31G(d,p)).¹

Compound	λ_{obsd} [nm]	λ_{calcd} [nm]	Oscillator strength
DTR	615	648	0.12
CN-DTR	587	635	0.21
Py-DTR	631	682	0.28
Ethynyl-DTR	654	720	0.35
Th-DTR	668	733	0.31
MeO-DTR	703	724	0.15

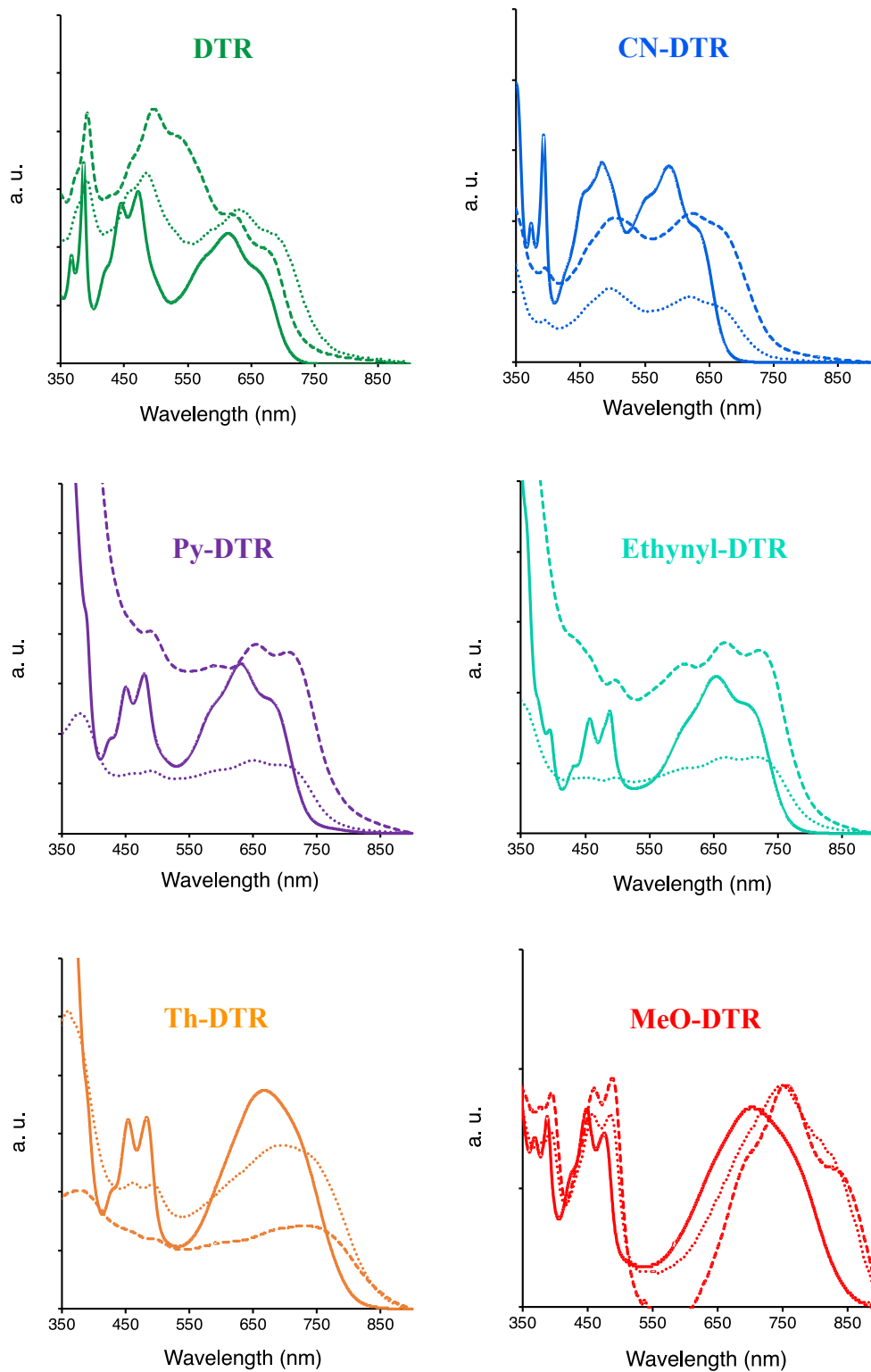


Figure S3. UV-Vis-NIR absorption spectra in thin film deposited by spin-coating (dotted lines) and drop-casting (dashed lines). Absorption spectra in solution are depicted in solid lines.

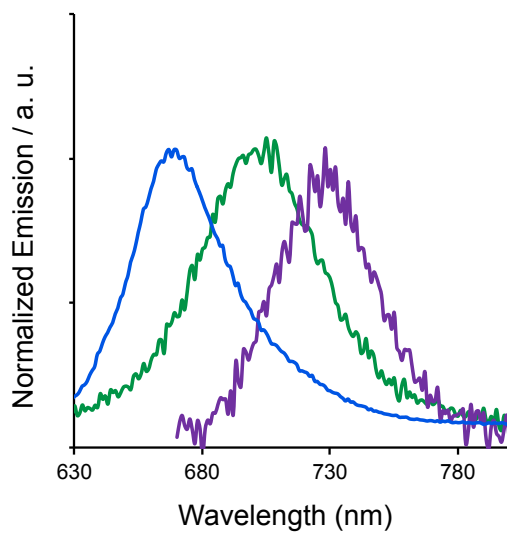


Figure S4. Normalized emission spectra of **DTR** (green line), **CN-DTR** (blue line), and **Py-DTR** (purple line) in CHCl_3 solution (10^{-4} M).

Table S3. Absorption maximum wavelengths and the fluorescence maximum wavelengths.

Compound	λ_{abs} [nm]	λ_{em} [nm]
DTR	615	702
CN-DTR	587	671
Py-DTR	631	728

Table S4. Reduction potentials.

Compound	$E_{\text{red(1st)}}^{1/2}$ [V]	$E_{\text{red(2nd)}}^{1/2}$ [V]	ΔE [V]
DTR	-1.56	-2.04	0.48
CN-DTR	-1.24	-1.60	0.36
Py-DTR	-1.42	-1.76	0.34
Ethynyl-DTR	-1.41	-1.81	0.40
Th-DTR	-1.45	-1.88	0.43
MeO-DTR	-1.59	-2.09	0.50

Table S5. Comparison of electrochemical properties between the observed value and theoretical value estimated by DFT calculation (B3LYP/6-31G(d,p)).¹

Compound	$E_{\text{HOMO}}^{\text{obsd}}$ [eV]	$E_{\text{HOMO}}^{\text{calcd}}$ [eV]	$E_{\text{LUMO}}^{\text{obsd}}$ [eV]	$E_{\text{LUMO}}^{\text{calcd}}$ [eV]	E_g^{obsd} [eV]	E_g^{calcd} [eV]
DTR	(-5.07)	-5.04	-3.24	-2.66	(1.83)	2.38
CN-DTR	-5.82	-5.82	-3.56	-3.45	2.26	2.37
Py-DTR	-5.37	-5.24	-3.38	-2.98	1.99	2.26
Ethynyl-DTR	(-5.05)	-5.01	-3.39	-2.89	(1.66)	2.12
Th-DTR	-5.06	-4.87	-3.35	-2.77	1.71	2.1
MeO-DTR	-4.77	-4.74	-3.21	-2.57	1.56	2.17

S3. OFET characteristics

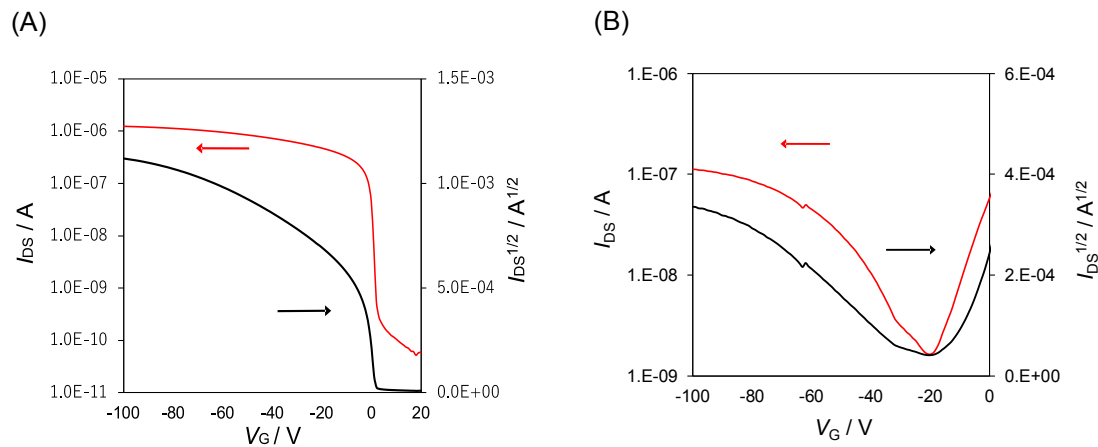


Figure S5. Transfer plots of (A) **OD-MeO-DTR** and (B) **OD-CN-DTR**-based OFET device fabricated on HMDS-treated SiO_2 insulation surface in an as-cast film.

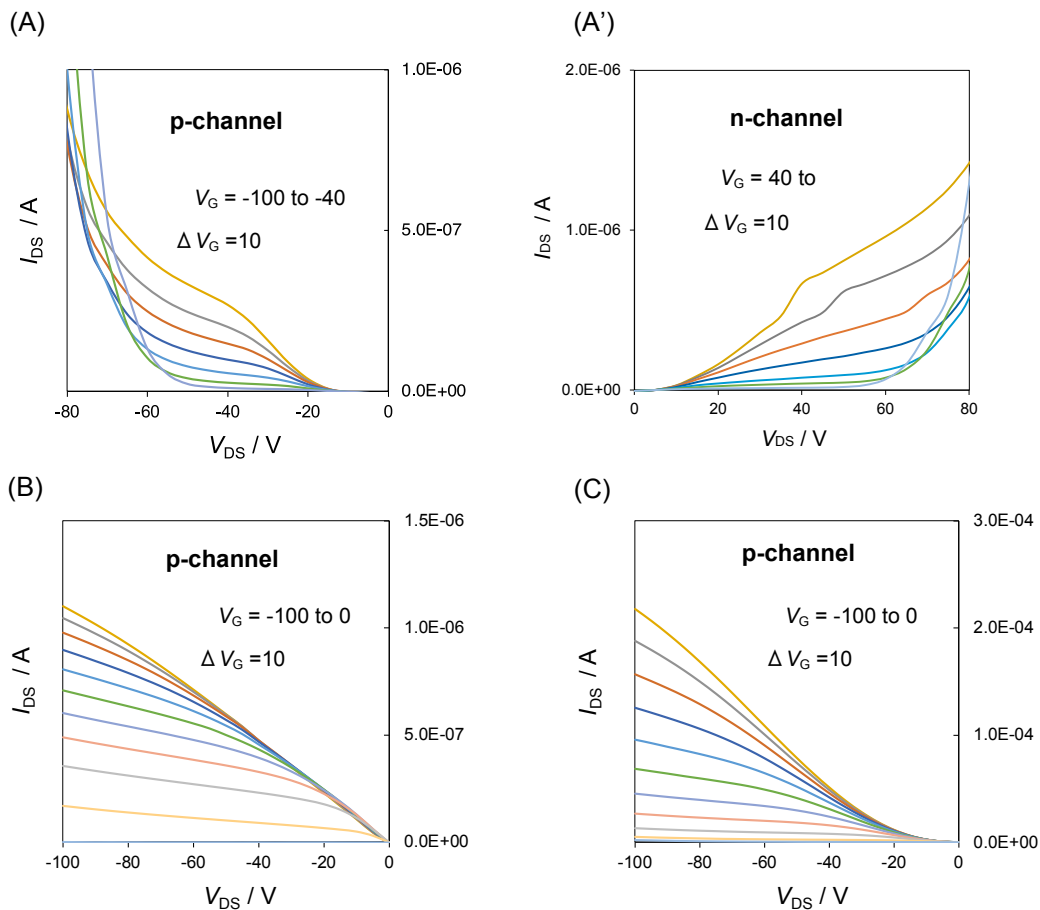


Figure S6. Output plots of (A) and (A') **OD-CN-DTR** [annealed at 100 °C], (B) **OD-MeO-DTR** [as-cast], and (C) **EH-MeO-DTR** [annealed at 100 °C]-based OFET device fabricated on HMDS-treated SiO_2 insulation surface.

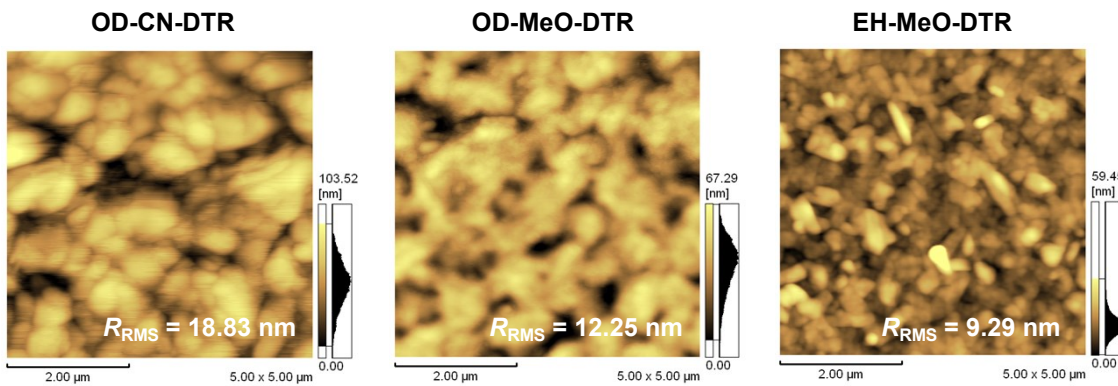


Figure S7. AFM image ($5 \mu\text{m} \times 5 \mu\text{m}$) of the films fabricated on HMDS-treated SiO_2 insulation surface. The inset values indicate the root-mean-square roughness (R_{RMS}).

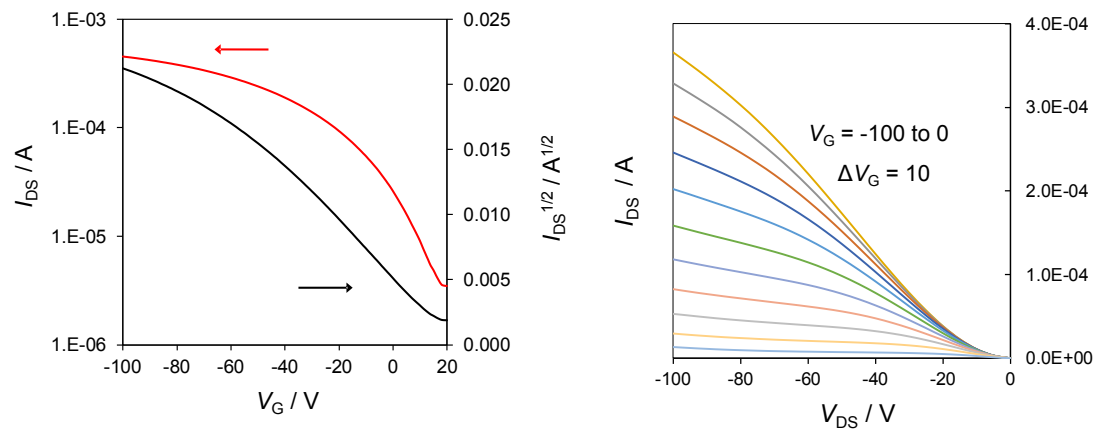


Figure S8. Transfer (left) and output (right) curves of **EH-MeO-DTR**-based OFET device fabricated on HMDS-treated SiO_2 insulation surface using Au electrodes modified with 1-hexadecanethiol.

S4. OPV characteristics

Table S6. OPV characteristic with the device architecture ITO/ZnO/P3HT:**OD-CN-DTR/MoO₃**/Ag.

solv.	conc. [mg/mL]	PCE [%]	J_{sc} [mA/cm ²]	V_{oc} [V]	FF [%]
chlorobenzene	20	0.21	0.84	0.56	44
chloroform	10	0.10	0.59	0.40	43

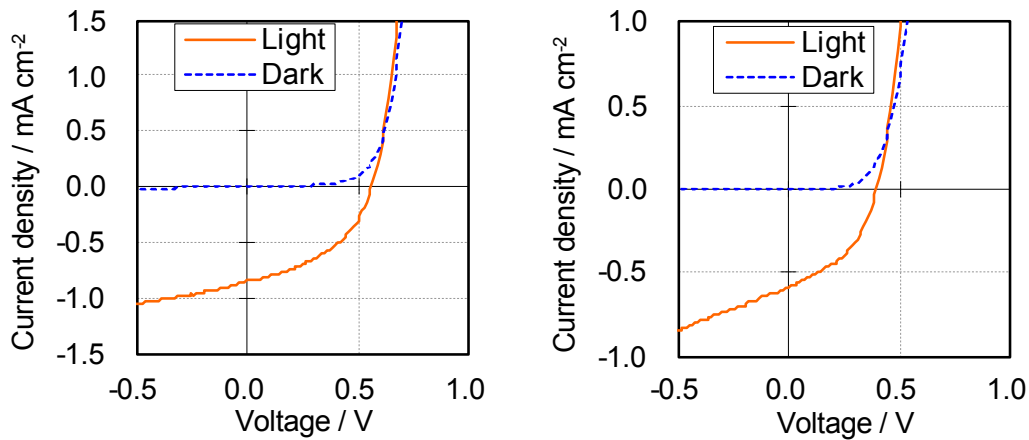


Figure S9. J - V curve for ITO/ZnO/P3HT:**OD-CN-DTR/MoO₃**/Ag device. The active layer was fabricated from chlorobenzene (left) and chloroform (right) solutions.

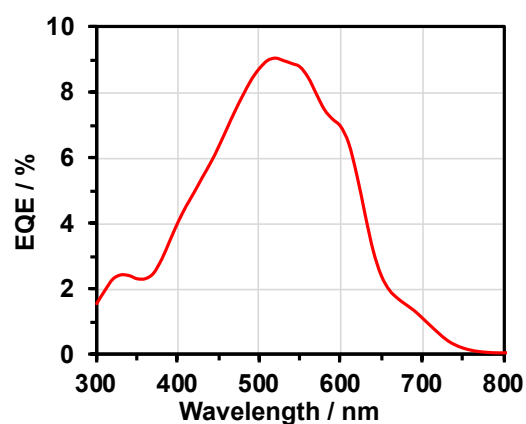


Figure S10. EQE spectrum for ITO/ZnO/P3HT:**OD-CN-DTR**/MoO₃/Ag device, in which the active layer was fabricated from chlorobenzene solution.

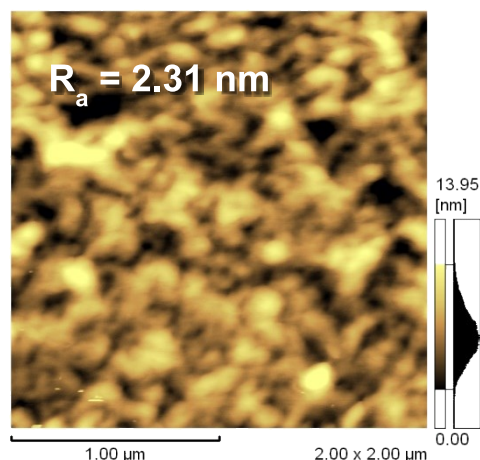
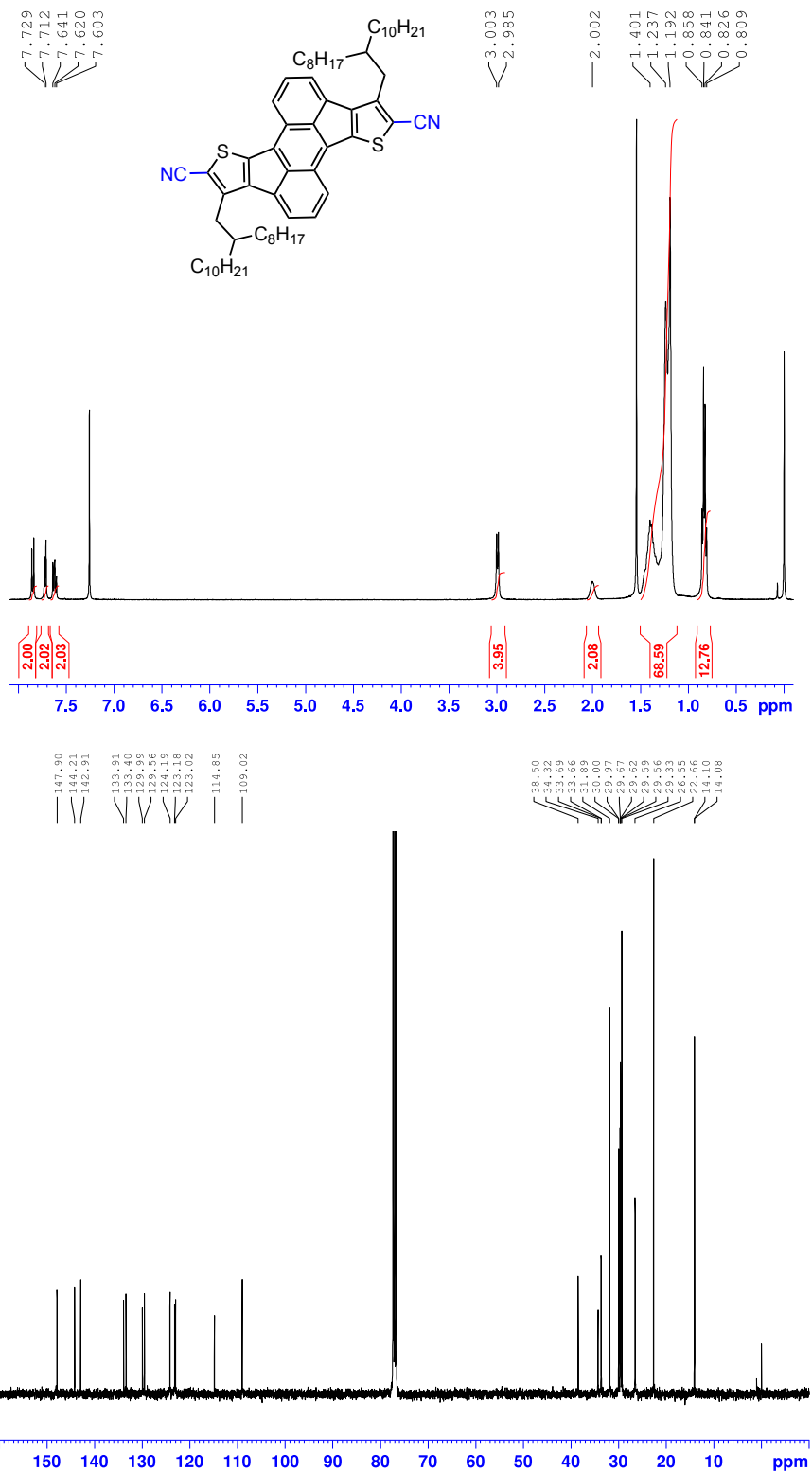


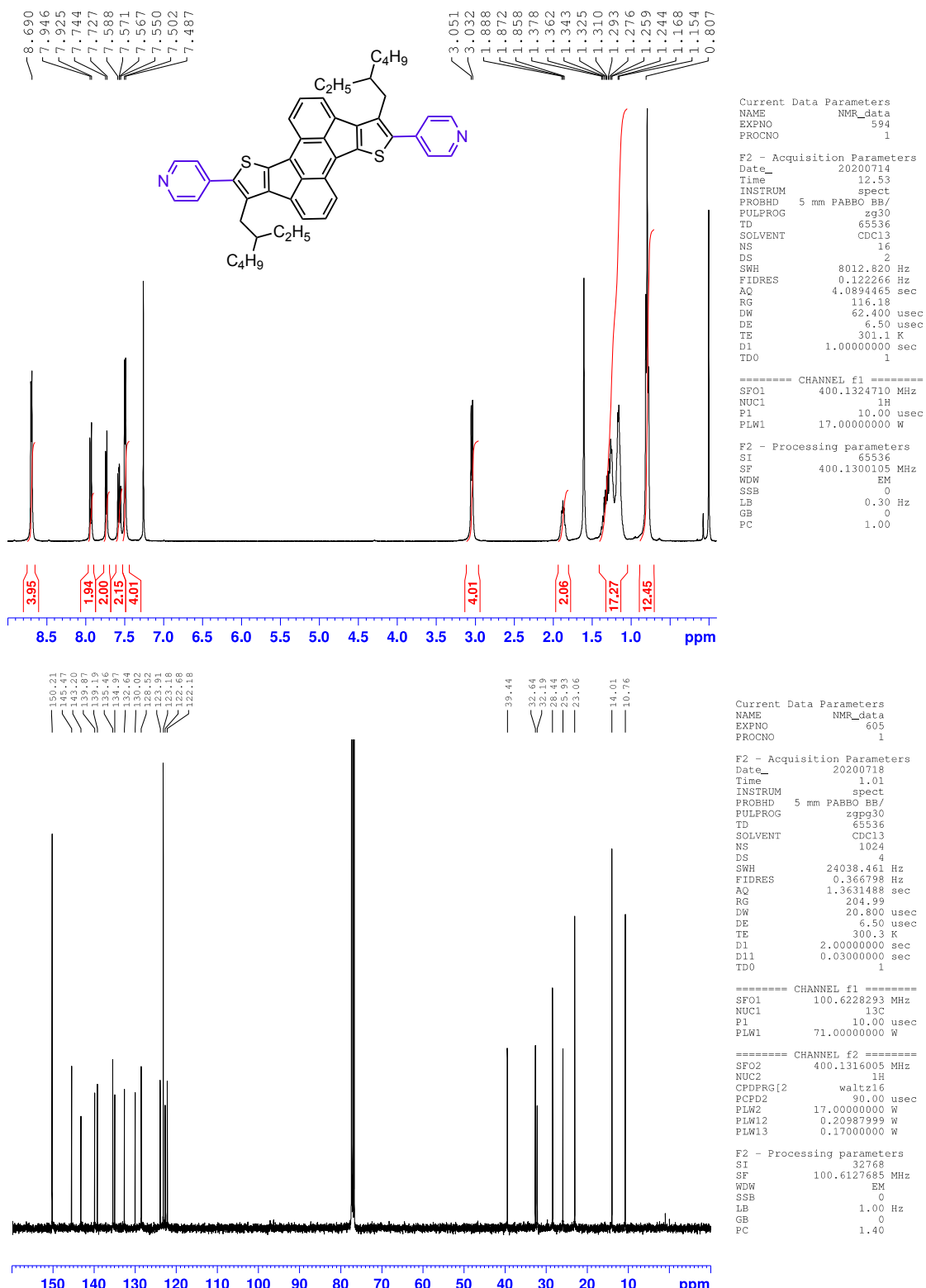
Figure S11. AFM image of the active layer.

S5. NMR spectra OD-CN-DTR

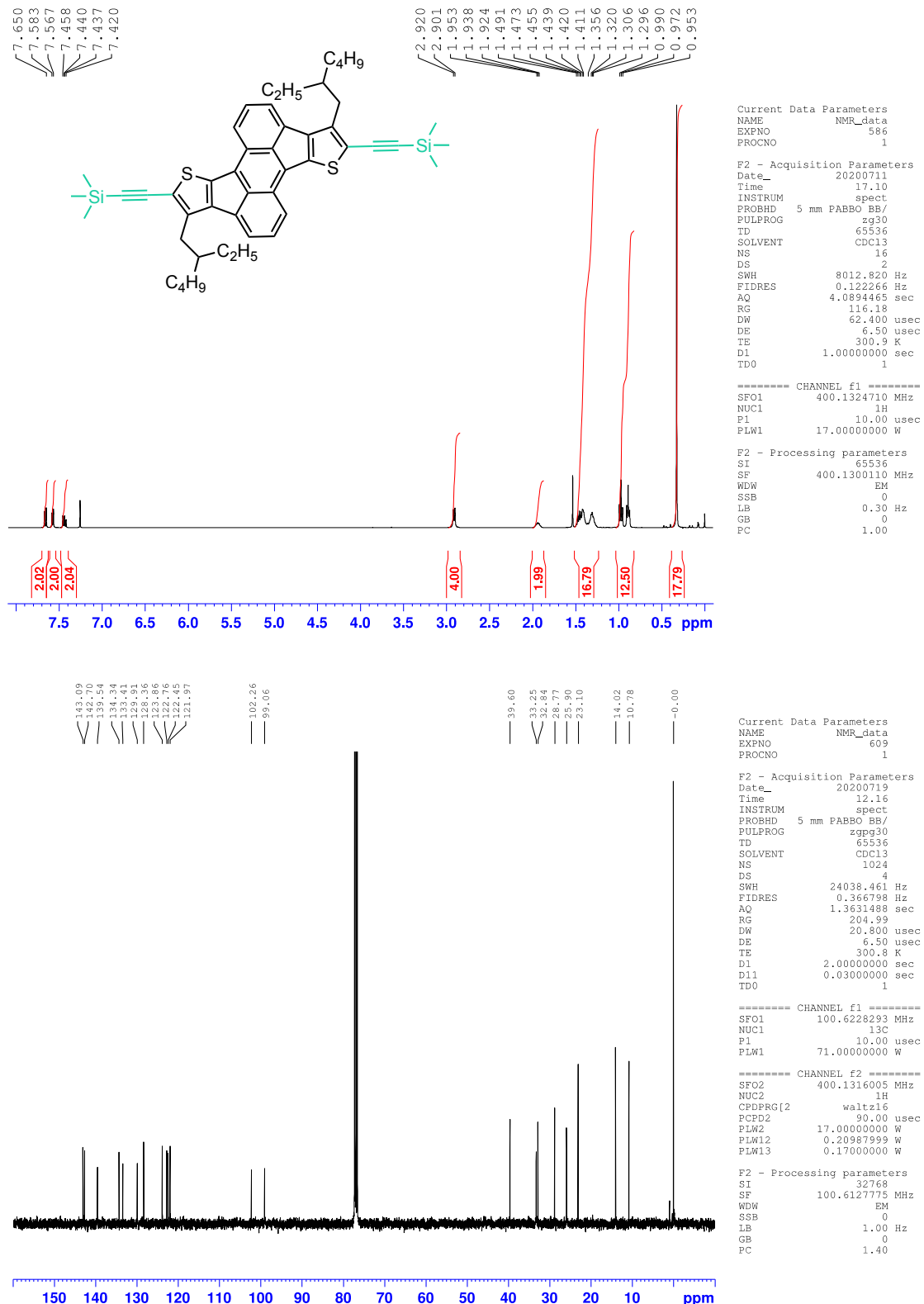


12

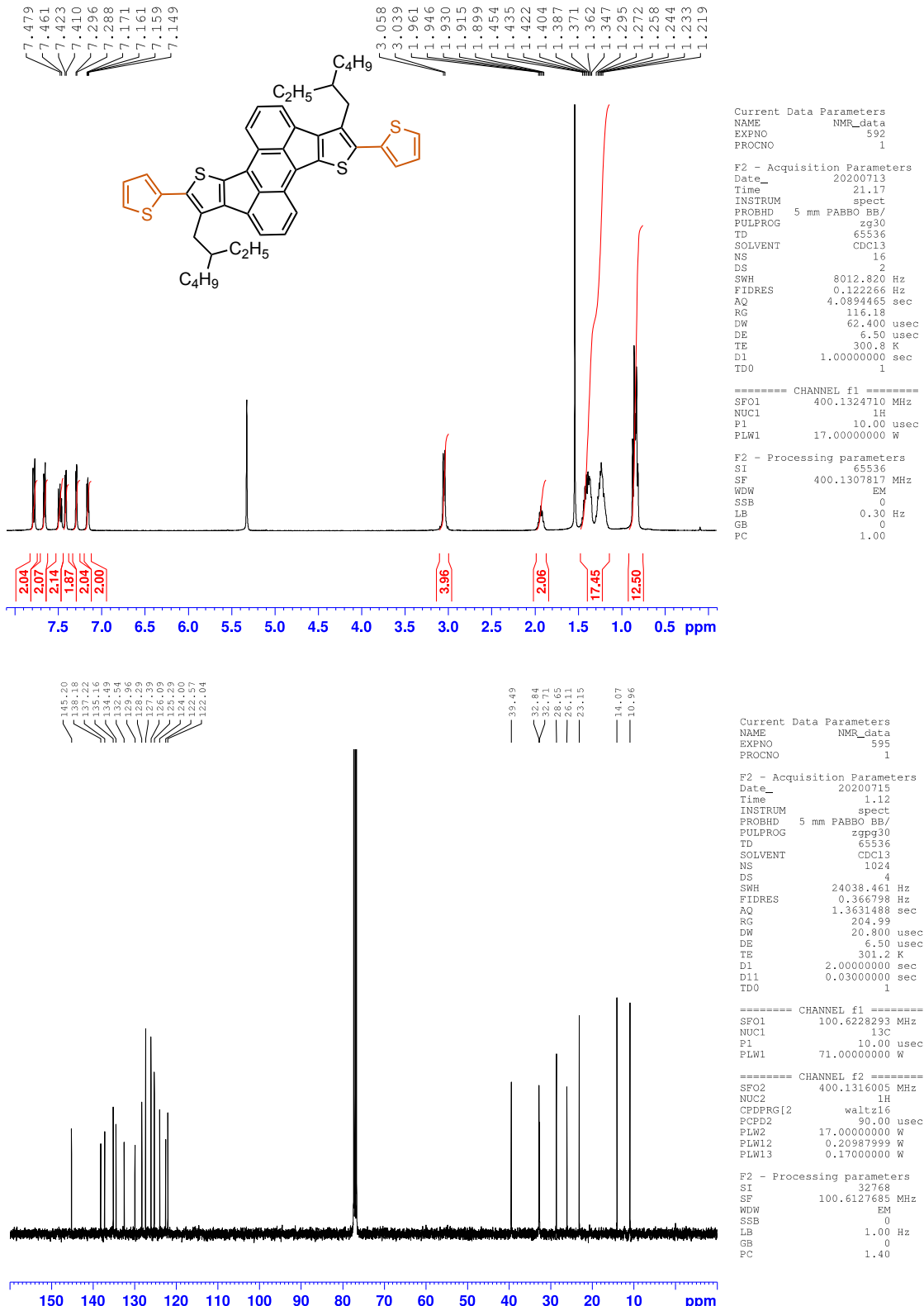
EH-Py-DTR



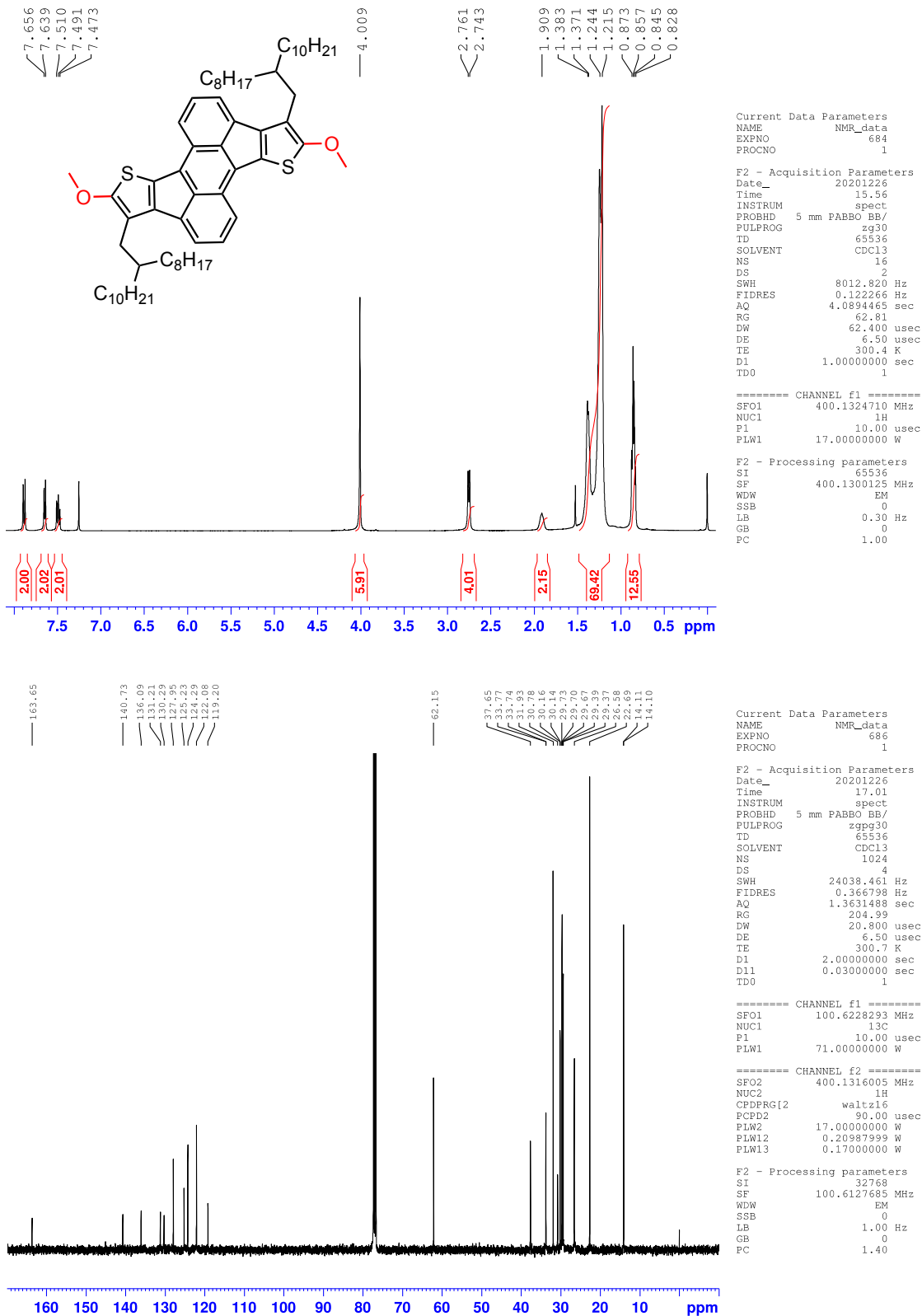
EH-Ethynyl-DTR



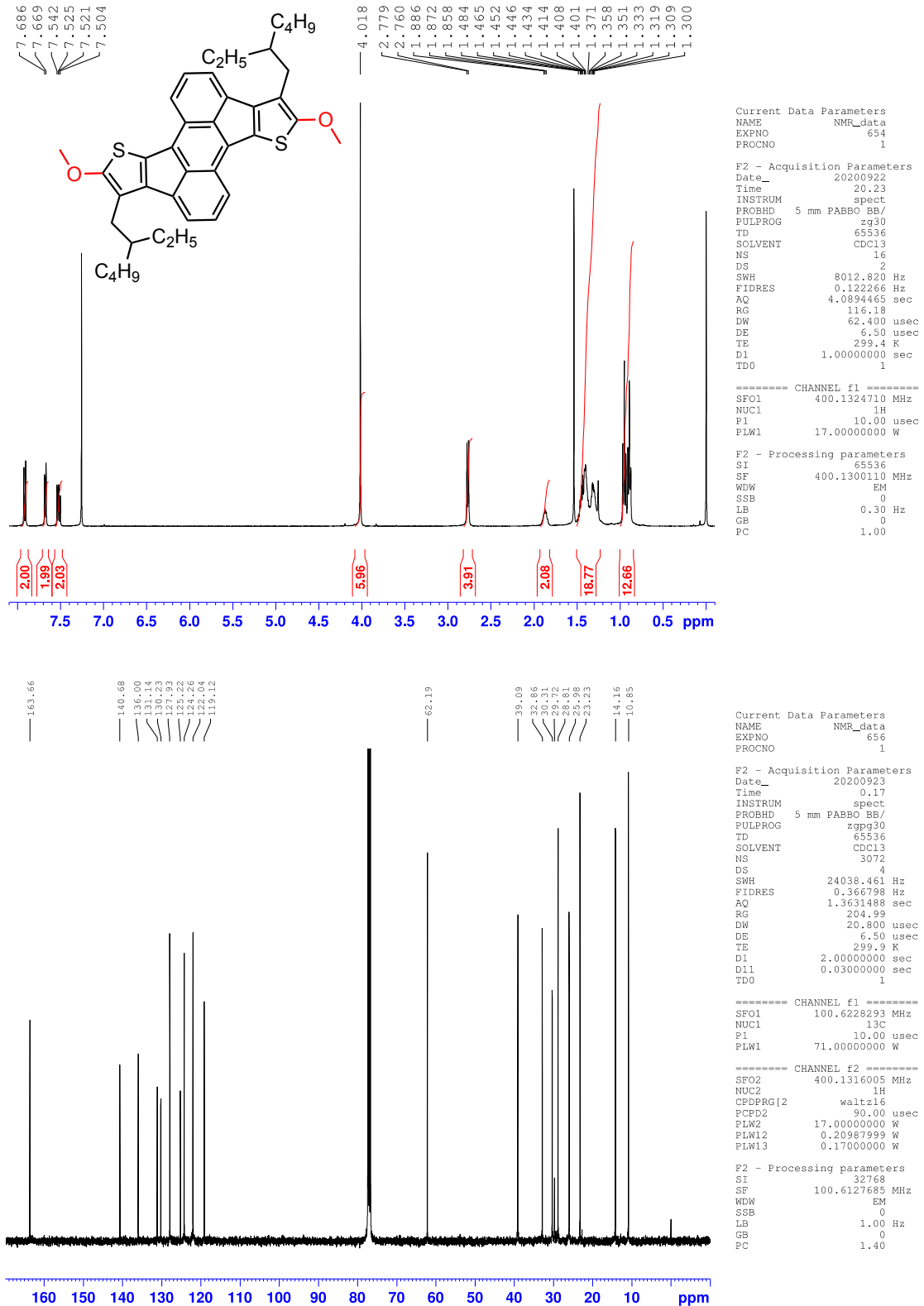
EH-Th-DTR



OD-MeO-DTR



EH-MeO-DTR



S6. Reference

- 1) Gaussian 09, Revision E.01, M. J. Frisch, G. W. Trucks, H. B. Schlegel, G. E. Scuseria, M. A. Robb, J. R. Cheeseman, G. Scalmani, V. Barone, B. Mennucci, G. A. Petersson, H. Nakatsuji, M. Caricato, X. Li, H. P. Hratchian, A. F. Izmaylov, J. Bloino, G. Zheng, J. L. Sonnenberg, M. Hada, M. Ehara, K. Toyota, R. Fukuda, J. Hasegawa, M. Ishida, T. Nakajima, Y. Honda, O. Kitao, H. Nakai, T. Vreven, J. A. Montgomery, Jr., J. E. Peralta, F. Ogliaro, M. Bearpark, J. J. Heyd, E. Brothers, K. N. Kudin, V. N. Staroverov, T. Keith, R. Kobayashi, J. Normand, K. Raghavachari, A. Rendell, J. C. Burant, S. S. Iyengar, J. Tomasi, M. Cossi, N. Rega, J. M. Millam, M. Klene, J. E. Knox, J. B. Cross, V. Bakken, C. Adamo, J. Jaramillo, R. Gomperts, R. E. Stratmann, O. Yazyev, A. J. Austin, R. Cammi, C. Pomelli, J. W. Ochterski, R. L. Martin, K. Morokuma, V. G. Zakrzewski, G. A. Voth, P. Salvador, J. J. Dannenberg, S. Dapprich, A. D. Daniels, O. Farkas, J. B. Foresman, J. V. Ortiz, J. Cioslowski, and D. J. Fox, Gaussian, Inc., Wallingford CT, 2013.